ELSEVIER

Journal of Structural Geology 28 (2006) 1994–2010

JOURNAL OF STRUCTURAL GEOLOGY

www.elsevier.com/locate/jsg

Accommodation of compressional inversion in north-western South Island (New Zealand): Old faults versus new?

F.C. Ghisetti*, R.H. Sibson

Department of Geology, University of Otago, PO Box 56, Dunedin, New Zealand

Received 30 March 2005; received in revised form 2 June 2006; accepted 5 June 2006
Available online 22 August 2006

Abstract

In the NW South Island, New Zealand, high-angle faults inherited from episodes of Late Cretaceous–Paleocene and Eocene extension have, since the early Miocene, undergone compressional inversion in association with right-lateral shearing and transpression on the Alpine Fault. Active reverse faulting and large historical earthquakes occur along N–S to NNE–SSW trending faults which at the surface dip 45–75° to both the east and west. The faults truncate subparallel folds that deform the Tertiary sequence overlying a composite Paleozoic–Mesozoic crystalline basement. However, the deep geometry of these faults, their penetration into the middle-to-lower crust and their relationship to the Alpine Fault are poorly understood. The tectonic architecture of this compressional inversion province is analysed by reconstructing structural contours at the base of the Oligocene carbonate sequence in the north-west of the South Island. Deformation of the Oligocene carbonate sequence, structural analyses in the field and subsurface data indicate a mixed style of inversion with (1) reactivation of some high-angle normal faults and (2) thrusting on new, moderate-dipping cross-cutting faults that detach slivers of basement and cause flexural folding in the sedimentary cover. These faults may remain blind or concealed beneath cover sequences but are likely to control seismic rupturing in the basement at depths of ~10–15 km.
© 2006 Elsevier Ltd. All rights reserved.

Keywords: Normal faults; Thrusts faults; Folds; Inversion tectonics; New Zealand

1. Introduction

The crustal architecture of the South Island of New Zealand is dominated by lithological and structural heterogeneities, inherited from a complex sequence of tectonic events. Following collision and accretion of Terranes on the Gondwana margin during the Tuhua (Devonian–Carboniferous) and Rangitata (Jurassic–Early Cretaceous) orogenies (Bishop et al., 1985), the continental block of New Zealand separated from Australia and Antarctica during episodes of Middle–Late Cretaceous and Late Cretaceous–Paleocene rifting in the Tasman Sea (Nathan et al., 1986). Spreading halted in the Late Paleocene (c. 56 Ma), but a new extensional plate boundary was initiated at c. 45 Ma across the South East Tasman and Emerald Basins (Fig. 1), and propagated into continental crust on the western margin of the South Island (Lebrun et al., 2003). In the late Eocene–Oligocene, an alignment of extensional basins extended across the whole length of the South Island and in the Taranaki region (King, 2000). During the time interval 25–20 Ma, a change in orientation of the Pacific–Australia plate motion vector initiated the processes of oblique compression across the plate boundary (Sutherland, 1995). Timing of the inception of the Alpine Fault remains controversial (see Sutherland, 1999 for a discussion), but plate reconstructions (e.g. Sutherland, 1995; King, 2000) constrain the establishment of a through-going right-lateral transform to around 25 Ma (late Oligocene–Early Miocene), with a progressive increase in convergence rates since the late Miocene (10 Ma).

With average strike-slip rates of 25–30 mm year^{-1} the Alpine Fault has taken up 60–80% of the Australia–Pacific

* Corresponding author. Tel.: +64 03 4799051; fax: +64 03 4797527.
E-mail address: francesca.ghisetti@otago.ac.nz (F.C. Ghisetti).

0191-8141/$ - see front matter © 2006 Elsevier Ltd. All rights reserved.
doi:10.1016/j.jsg.2006.06.010

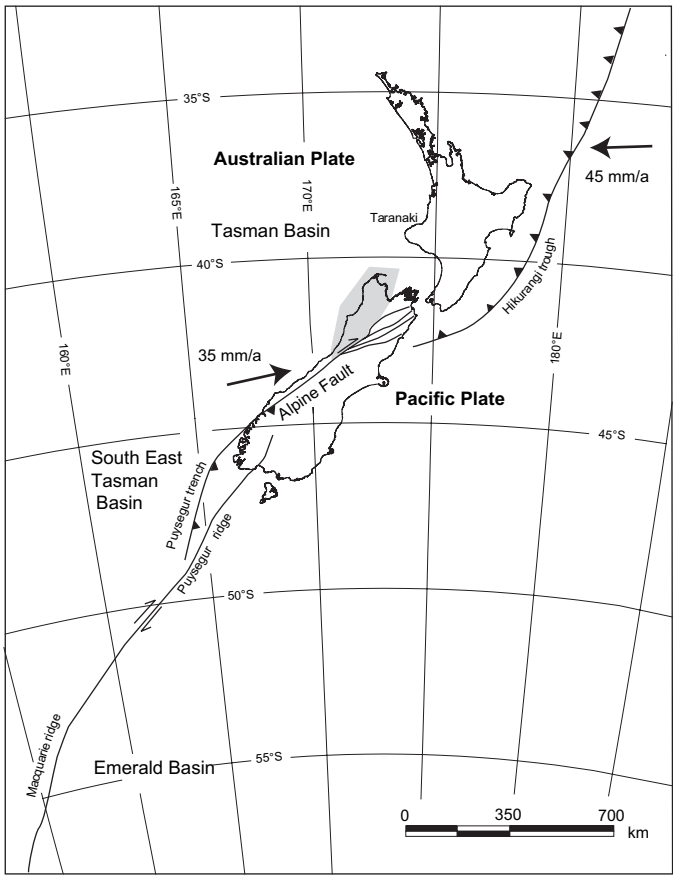

Fig. 1. Regional setting of the study area (in light grey) relative to the transpressive Australia–Pacific plate margin in the South Island and the Alpine Fault. Interplate slip vector from Nuvel 1A model of DeMets et al. (1994).

lateral motion in the last 5 Ma (Figs. 1 and 2). In contrast, dip slip rates vary significantly along strike (from 2 to 8 mm year^{-1}; cf. Norris and Cooper, 2000) on fault segments dipping 45–70° SE. Thus, a significant fraction of the plate-perpendicular shortening is not accommodated along the Alpine Fault and is likely partitioned onto an array of other faults and folds.

Quaternary strike-slip and thrust faulting (Norris and Cooper, 1995, 2000) and GPS data (e.g. Holt and Haines, 1995; Beavan and Haines, 2001) indicate accumulated and ongoing deformation over a wide area in the hanging-wall of the Alpine Fault, consequent on crustal thickening within the Pacific plate in the convergent collisional orogen of the Southern Alps (Norris et al., 1990).

In contrast, deformation of the Australian plate is generally regarded as being of lower intensity, with passive flexuring and underthrusting along the west margin of the South Island (e.g. Koons, 1990). However, accommodation of shortening in the Australian plate west of the Alpine Fault is well testified by Neogene inversion of Late Cretaceous and Eocene normal faults along the western margin of the South Island (Wellman, 1949; Bishop and Buchanan, 1995) and in the Taranaki Basin (King and Thrasher, 1996). In these regions, offshore seismic data and geological mapping on land (Nathan et al., 1986; Bishop, 1992a) show that high-angle, N–S faults have controlled—through multiple episodes of compressional inversion—localisation and progressive foundering of the Miocene–Pliocene siliciclastic basins, contemporaneous with activity on the Alpine Fault. In addition, the two largest earthquakes of the last century in the South Island (1929 Buller M_s 7.8, and 1968 Inangahua M_s 7.4) occurred in the region west of the Alpine Fault, and were generated by reverse faulting (with secondary components of left-lateral slip) on N–S fault planes, respectively dipping 45° east and west (Anderson et al., 1994; Doser et al., 1999). From inversion of focal mechanisms in the northern South Island Balfour et al. (2005) deduce a compressional contemporary stress field with the greatest compressive stress σ_1 subhorizontal and trending 295 ± 16°. Moderate to steeply dipping seismically active N–S faults therefore dip at high angles to σ_1, and are poorly oriented for frictional reactivation in the contemporary stress field (Sibson, 1990). A number of studies have focused on different structural characteristics of the deformed Australian crust (e.g. Berryman, 1980; Lihou, 1993; Anderson et al., 1994; Pettinga and Wise, 1994; Bishop and Buchanan, 1995; Kamp et al., 1996; Yeats, 2000; Nicol and Nathan, 2001), but the percentage of plate-perpendicular shortening partitioned onto faults in the Australian crust is largely unquantified. In fact it remains unclear whether deformation is distributed through a large network of faults or is associated with reactivation of a few master faults with very long recurrence intervals (e.g. Anderson et al., 1993).

Understanding selectivity of fault reactivation and slip partitioning in an array of faults are problems common to many inversion provinces (e.g. Buchanan and Buchanan, 1995). The South Island of New Zealand offers favourable conditions to address these problems because of the well-documented sequence of syntectonic sedimentary events (Nathan et al., 1986), coupled to high rates of deformation in one of the most active oblique margins in the world.

The aim of this paper is: (1) to assess the fault geometry in the footwall of the Alpine Fault in the NW of the South Island; (2) to define the style of compressional deformation—thin-skinned detachments vs. fault penetration into the basement, and (3) to evaluate the partitioning of shortening between folding, reactivation of old faults, and creation of new faults. The analysis is based on the reconstruction of the structural contours of a key marker horizon (the base of the Oligocene carbonate sequence), and is complemented by structural analyses in selected key areas, and available seismic profiles and drillholes. Interpretation of these data is summarised in a regional cross-section that emphasizes the coexistence of inverted, steep faults inherited from earlier extensional phases, moderate-dipping blind thrust faults favourably oriented in the present stress regime, and layer-parallel detachments within folded sedimentary covers. The geometry of faulting in the lower-mid crust and structural connections to the Alpine Fault remain highly speculative, but analysis of available data and quantification of shortening suggest that blind thrusts, concealed beneath thick panels of detached sedimentary cover, may rupture in large earthquakes at 10–15 km depth. Given the short-term historical record of seismic activity in New Zealand,

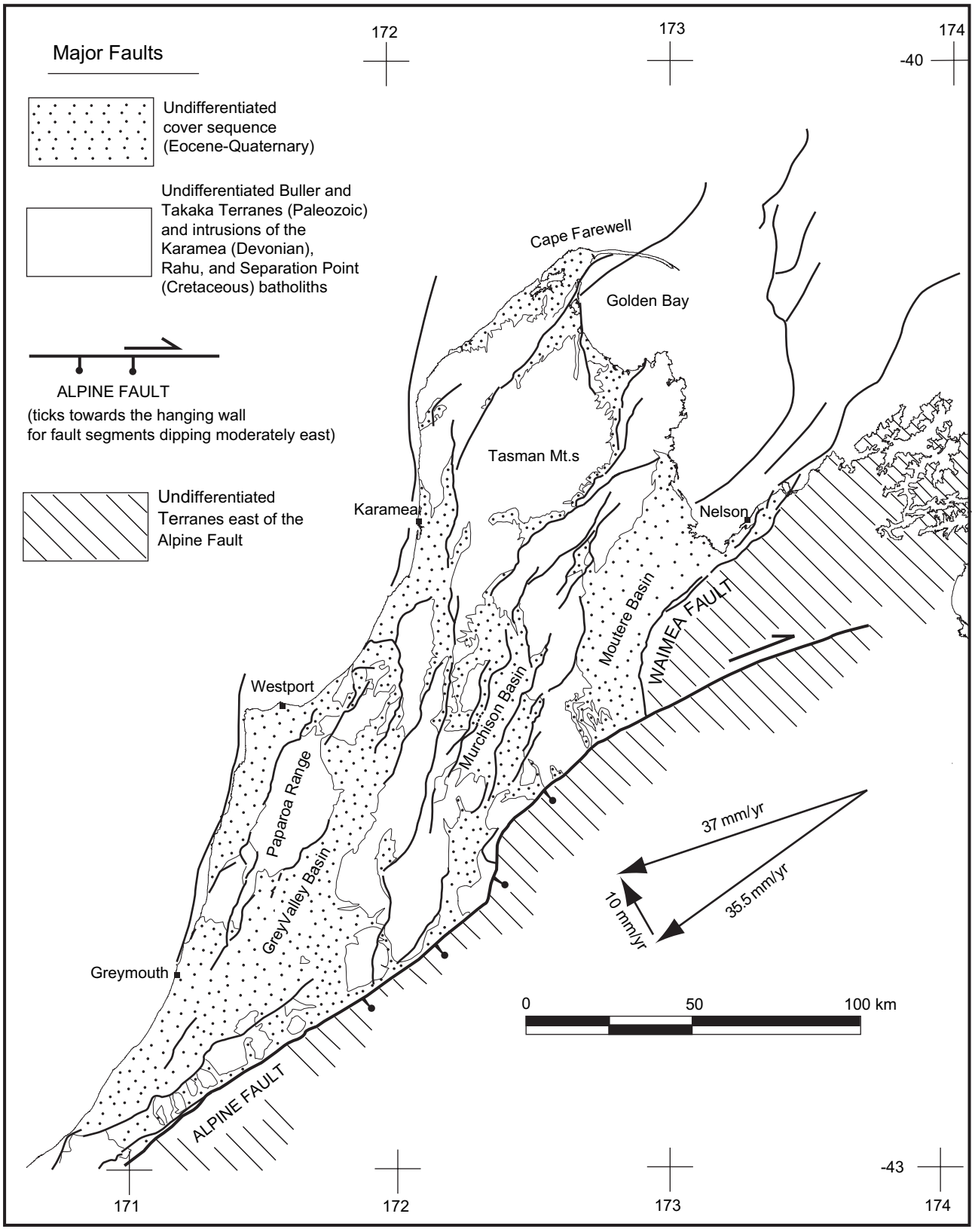

Fig. 2. Tectonic sketch map of the study area, in the footwall of the Alpine Fault. Redrawn and simplified from Nathan et al. (1986), Rattenbury et al. (1998) and Nathan et al. (2002). Partitioning of the interplate velocity vector parallel and perpendicular to the Alpine Fault after Norris and Cooper (2000).

seismogenic faults that have not ruptured in the past 200 years may still remain undetected.

2. Oligo–Miocene sedimentation and compressional tectonic inversion

The structural grain of the investigated region (Fig. 2) is dominated by an array of faults with dominant N–S to NNE–SSW orientation, some of which are inherited from the Late Cretaceous–Paleocene rifting in the Tasman Sea (Nathan et al., 1986; Bishop and Buchanan, 1995). Distribution of thick fluvio-lacustrine deposits (Paparoa Coal Measures, latest Cretaceous to Paleocene) and of coarse clastic deposits testifies to localised subsidence and strong vertical mobility, connected to the activity of basin-bounding master faults.

Following a period of Late Paleocene–Early Eocene subaerial erosion, with accumulation of fluvial-lacustrine deposits (Brunner Coal Measures), regional marine transgression started in the Middle Eocene (shallow water mudstones of the Kaiata Formation). The peak of post-rifting passive subsidence is marked by deposition of a marine calcareous sequence (Nile Group) during the Oligocene (34–27 Ma). Facies of the Oligocene sequence (from shallow water bioclastic limestones to deeper water basinal calcareous mudstones) and thickness variations (<100 m thick condensed sequence in stable platforms and ≤1000 m thick calcareous mudstones in subsiding basins; cf. Nathan et al., 1986) are indicative of a complex paleogeographic setting, likely related to persistent structural highs inherited from the rifted margin and/or synsedimentary tectonics. Available reconstructions (Nathan et al., 1986; King et al., 1999) define a large shelf area (paleodepths of 50–200 m), segmented by deeper basins (Paparoa and Murchison basins, Fig. 3a). Although paleogeographic reconstructions suggest that a large part of New Zealand was submerged during the Oligocene, a number of paraconformities and unconformities occur in the sequence, and have been interpreted as resulting from basin starvation or removal of sediments by submarine current erosion (e.g. ''Marshall paraconformity'' at 29 Ma; see Carter, 1985).

Starting with the Early Miocene, localisation of rapidly subsiding syntectonic basins infilled by terrigenous sequences and a regional unconformity track a dramatic change in vertical mobility, and mark the onset of compressional deformation that continues today. These episodes are related to the reorganisation of the Australian–Pacific convergent plate boundary, with progressive accumulation of right-lateral slip and oblique transpression on the Alpine Fault and uplift of the Southern Alps (Sutherland, 1995; King, 2000).

Progressive differential uplift is recorded by the Miocene to Pliocene regressive syntectonic clastic sequence (Lower and Upper Blue Bottom Group), which exhibits strong lateral variations in facies and thickness, and a number of unconformities. In the study area the Lower Blue Bottom Group concordantly overlies the Oligocene carbonates when deposited in persistently subsiding basins (e.g. Murchison basin), but lies unconformably above the basement of the Eocene units (e.g. wells Haku 1, Kawhaka 1, and Hokitika area; cf. Nathan et al., 1986) when deposited above blocks that underwent a reversal in mobility during the episodes of shortening.

3. Structural contour map of the base of the Oligocene sequence

3.1. Methods and problems

The calcareous Oligocene sequence is a convenient marker for assessing amounts and gradients of regional deformation because it was deposited over a wide area at the end of rifting and immediately before the onset of compressional tectonics. Structural contour maps of the high energy reflector at the base of the Oligocene calcareous sequence calibrated from seismic lines and tied to exploration wells are available for the Taranaki Basins (Nathan et al., 1986; King and Thrasher, 1996) and the subsurface of the Grey Valley Basin (New Zealand Oil and Gas, 1997), but no regional structural contour map of the Oligocene sequence exposed on land has previously been compiled. Note, however, that the ''base'' of the Oligocene sequence is a time-transgressive horizon that was not deposited as a flat, equipotential surface.

Time progression of the Oligocene transgression does not affect the structural interpretations because compressional deformation started during the Early Miocene and became progressively accentuated during the Pliocene and Quaternary. Original paleodepths variations are more important, because in the investigated area a large shelf domain (depth of 50–200 m) was transitional to a basinal domain centred in the Paparoa and Murchison troughs (cf. Fig. 3.21 in Nathan et al., 1986 and Fig. 3a).

Structural contours at the base of the Oligocene sequence (Fig. 3b and c) have been interpolated by: (i) plotting the elevation of the outcropping base of the Nile Group mapped in the Nelson and Greymouth 1:250,000 digital maps (Rattenbury et al., 1998; Nathan et al., 2002); (ii) extrapolating the base of the Oligocene above and below surface, using published cross-sections (Rattenbury et al., 1998; King and Thrasher, 1996) and a series of new, closely spaced cross-sections; and, (iii) incorporating public domain subsurface data (Janssen, 1963; Flandin, 1967; Petroleum Corporation of New Zealand, 1984; Nathan et al., 1986; Bishop, 1992a; Lihou, 1993; Bishop and Buchanan, 1995; King and Thrasher, 1996; New Zealand Oil and Gas, 1997).

Contours were originally compiled at vertical intervals of 100 m, but for clarity they have been redrawn at 500 m contour interval in Fig. 3b and c.

Elevations are given relative to present sea level. However, deposition of the Oligocene sequence occurred during important sea level fluctuations between 34 and 29 Ma. There is no general consensus on eustatic curves for the Oligocene, but recent recalibrations (e.g. Hardenbol et al., 1998) indicate a sea level 200 m higher than today from 33 to 29 Ma, a consistent sea level fall (−30 m) at nearly 29 Ma and a sea level 60 ± 10 m higher than present from 27 to 25 Ma.

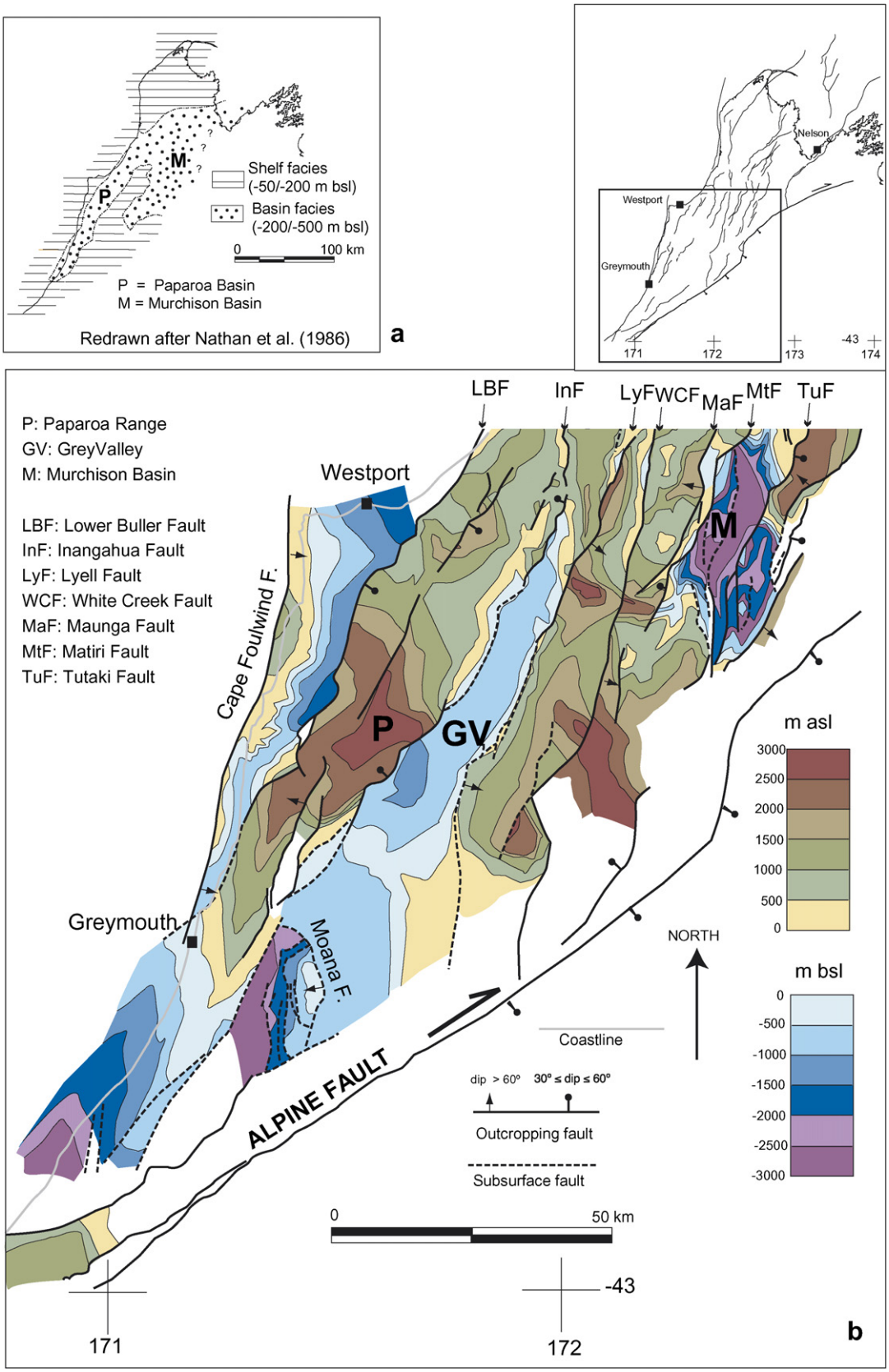

Fig. 3. (a) Paleogeographic reconstruction of the platform and basinal facies of the Oligocene carbonate sequence at time of deposition. (b) Structural contour map of the base of the Oligocene carbonate sequence for the southern part of the study area (regional location in inset). (c) Structural contour map of the base of the Oligocene carbonate sequence for the northern part of the study area. (Murchison basin (M) lies in the overlap region between the two maps; regional location in inset). Offshore data from King and Thrasher (1996).

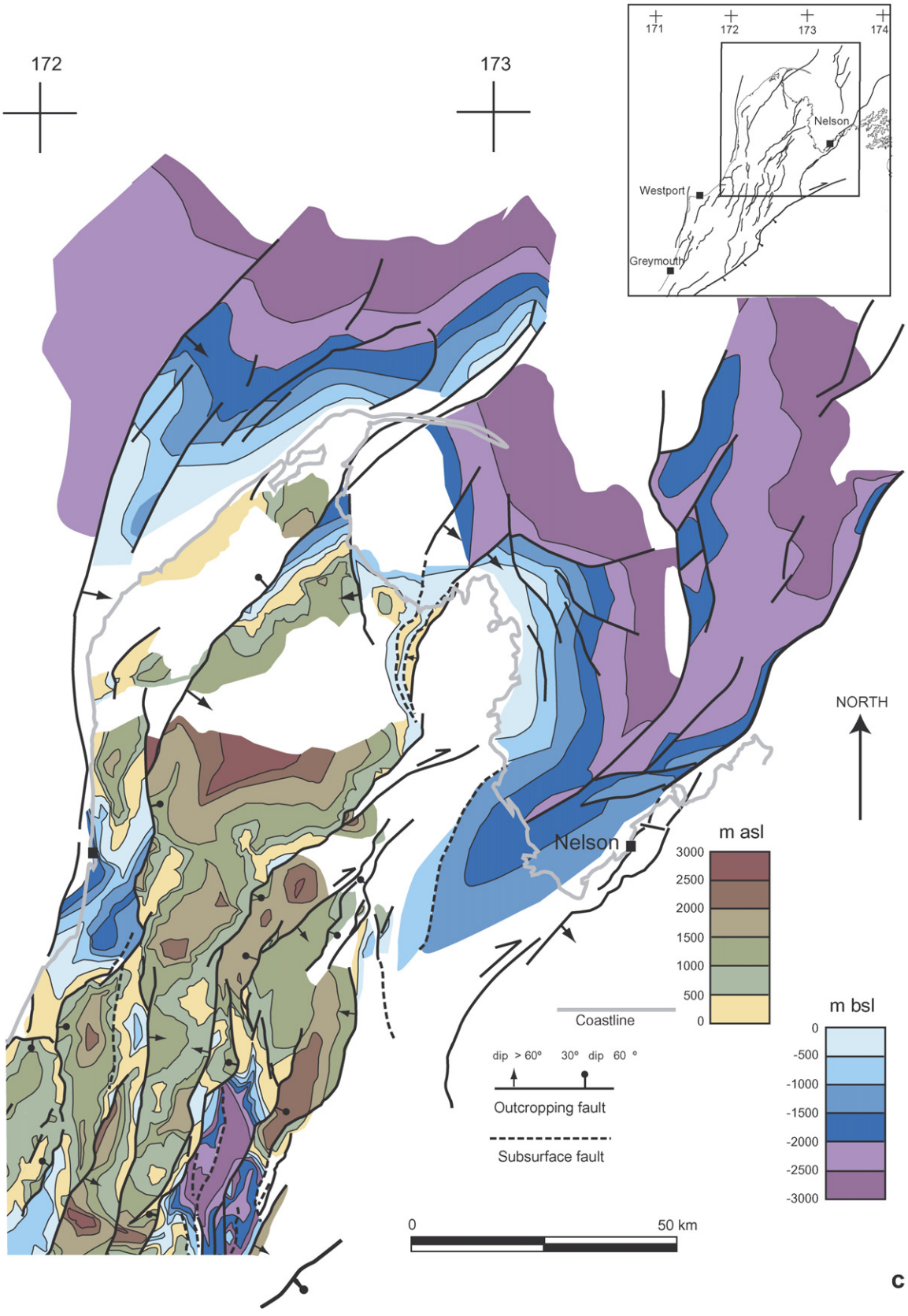

Fig. 3 (*Continued*)

3.2. Deformation of the base of the Oligocene sequence

Fig. 3b and c show the finite elevation of the Oligocene marker that results from shortening by folding and faulting since the Early Miocene. Some caution must be applied when considering the absolute elevations, because: (1) the original depositional surface was located at different depths (from 50 to 200 m bsl in the shelf areas to ≤500 m bsl in the basinal areas, Fig. 3a); (2) no eustatic correction has been applied; and (3) the rate and polarity of vertical movements have not necessarily been steady since deposition of the Oligocene marker. Thus, the structural contours of the base of the Oligocene cannot be directly transposed into slip rates.

The base of the Oligocene sequence is deformed with dominant N–S to NNE–SSW trends imparted by sets of folds, truncated on their limbs and cores by subparallel reverse faults (Fig. 3b and c). Axial traces of individual folds generally maintain continuity for up to 30–50 km. Adjacent fold pairs are often interconnected by steep flanks, eventually indicative of flexural shearing above buried faults (e.g. eastern flank of the Grey Valley syncline, Fig. 3b). The geometry of folds is consistent with concentric to chevron structures mapped in the field (see also Lihou, 1993), and moderate to steeply dipping axial surfaces. The anticlinal cores are uplifted blocks of denudated basement or inverted Cretaceous–Eocene basins (Bishop and Buchanan, 1995). Paleodepths of the Oligocene deposits in what are now the Paparoa and Lower Buller inverted basins were ≤500 m. Thus, present elevations of up to 2000–3000 m (Fig. 3b) give a minimum estimate of the finite uplift. The down-warped areas have the geometry of synsedimentary synclines (e.g. Grey Valley, Murchison, Fig. 3b and Karamea, Fig. 3a) that host the depocentres of the Miocene siliciclastic basins. All these basins were progressively shortened during Plio–Quaternary times as shown, for example, by the subsurface anticlines that deform thick Miocene sequences in the southern Grey Valley syncline (Moana Fault, Fig. 3b) and in the Murchison Basin (footwall of the Matiri and Tutaki Faults, Fig. 3b and c).

4. Faults that offset the base of the Oligocene sequence

The faults that offset the base of the Oligocene sequence are mapped in Fig. 4a. Fault orientation is almost exclusively N–S to NNE–SSW, with a peak for fault segments oriented at 20–50° to the Alpine Fault (Fig. 3b). Length of individual fault segments ranges from a few kilometres to up to 70–80 km, but segments are interconnected in defining structural alignments continuous for over 100 km.

The dip of individual faults has been assessed from maps and outcrops and—in only a few cases—from seismic lines (Bishop and Buchanan, 1995). Faults have accordingly been grouped in two broad classes of "moderate" and "steep" dips ($30° \leq \text{dip} \leq 60°$ and $\text{dip} > 60°$, see Fig. 3c). Truncation and offset of the Oligocene marker constrains reverse throws of 2000–3000 m along interconnected fault sets (Wakamarama–Kohaihai–Glasgow–Lower Buller, Inangahua–Maimai–Grey Valley, Pikikiruna–Maunga) and of 1500–2000 m along individual faults (Lyell, White Creek, Hohonu). Offshore, reverse throws ≥2000 m occur along fault planes steeply dipping east (Kahurangi–Kongahu and Cape Foulwind). Some fault segments (e.g. Inangahua and Maimai, southern end of the Lyell fault) are interconnected by steep planes of layer-parallel flexural slip that accommodate several hundred metres of vertical slip. This mechanism has been recognised in other regions of the Grey Valley syncline (Nicol and Nathan, 2001). Strong gradients in the structural contours of the Oligocene marker (Fig. 3b) possibly define blind, buried structures (e.g. east flank of the anticline in the hanging wall of the Inangahua Fault, Fig. 3c).

Previous work (e.g. Wellman, 1949; Ravens, 1990; Lihou, 1993; Bishop and Buchanan, 1995; Kamp et al., 1996; Rattenbury et al., 1998) has documented that the Kahurangi–Kongahu, Cape Foulwind, Wakamarama, Maunga, Matiri, and Grey Valley faults are all high-angle inverted normal faults inherited from the Late Cretaceous–Paleocene extensional phases, that have been reactivated with uplift and anticlinal folding of synextensional sedimentary basins in their hanging wall. Seismic lines published in Bishop (1992a) and Bishop and Buchanan (1995) show that in some cases compressional inversion occurred with simple reversal of motion on the same plane of the early normal fault (e.g. Cape Foulwind and Wakamarama Faults). In contrast, some field localities analysed in this study (localities a, b, c in Fig. 4) demonstrate that simple reactivation of the inherited normal fault did not always occur (Figs. 5 and 6). Unfortunately, the whole area offers few opportunities for detailed structural investigations, because of poor exposure and dense forest cover. In the case of the Pikikiruna Fault, outcrop and subsurface information help in constraining a complex geometry of fault reactivation (Fig. 5). Offshore seismic lines (Thrasher, 1989) show the anticlinal basement uplift east of the fault, but simple inversion of the pre-existing, NW-dipping normal fault is not feasible (see also King and Thrasher, 1996), because the synextensional Eocene coal measures, the Oligocene limestones and the syncompressional Miocene sequence remain downthrown in the fault hanging wall (Fig. 5a). At outcrop scale, the NW-dipping, high-angle planes of the Pikikiruna fault system display sets of oblique striations superposed onto normal striations (Fig. 5b), and are cross-cut by metre-scale, SE-dipping, reverse faults. An interpretation that integrates surface geology, small scale deformations, and subsurface geometry of thrusting in the Takaka Valley (see Ravens, 1990; Bishop and Buchanan, 1995) is shown in the cross-section of Fig. 5c, where the inherited, NW-dipping Pikikiruna normal fault is interpreted as truncated by a series of new, E-dipping reverse faults.

Truncation of the earlier, basin-bounding normal faults within the Eocene Buller coal basin can be inferred also from the regional setting in the Stockton coal mine (see Bishop, 1992b). In this area (locality b in Fig. 4), folded Eocene coal measures are overthrust by Paleozoic granites (Karamea Batolith) in the hanging wall of the W-dipping Mt. Frederick Fault on the west, and of the E-dipping

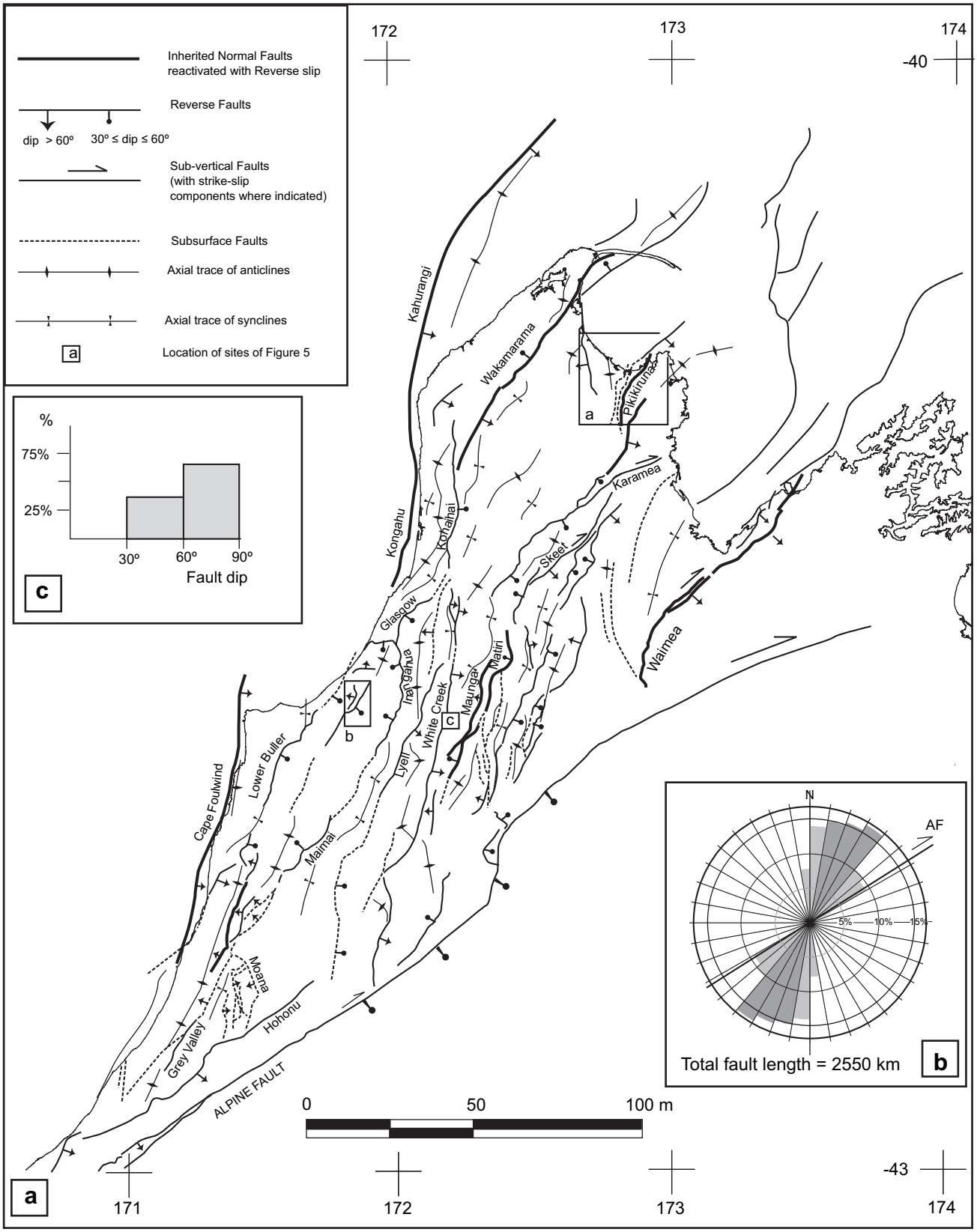

Fig. 4. (a) Major folds and faults that deform the base of the Oligocene sequence illustrated in Figs. 3b and c. Note that position and trend may not coincide with that of the outcropping structure. Subsurface faults are inferred from steep gradients of the structural contours (Fig. 3) or from available seismic lines (Nathan et al., 1986; Crundwell, 1990; Ravens, 1990; Buchanan, 1991; King and Thrasher, 1996; New Zealand Oil and Gas, 1997). Locality a is mapped in Fig. 5a, locality b is mapped in Fig. 6a and a structural detail of locality c is given in Fig. 6c. (b) Fault segment orientation relative to the Alpine Fault (AF), weighted by strike length. (c) Broad subdivision of faults in two dip classes, based on mapping, outcrop measurements and subsurface data.

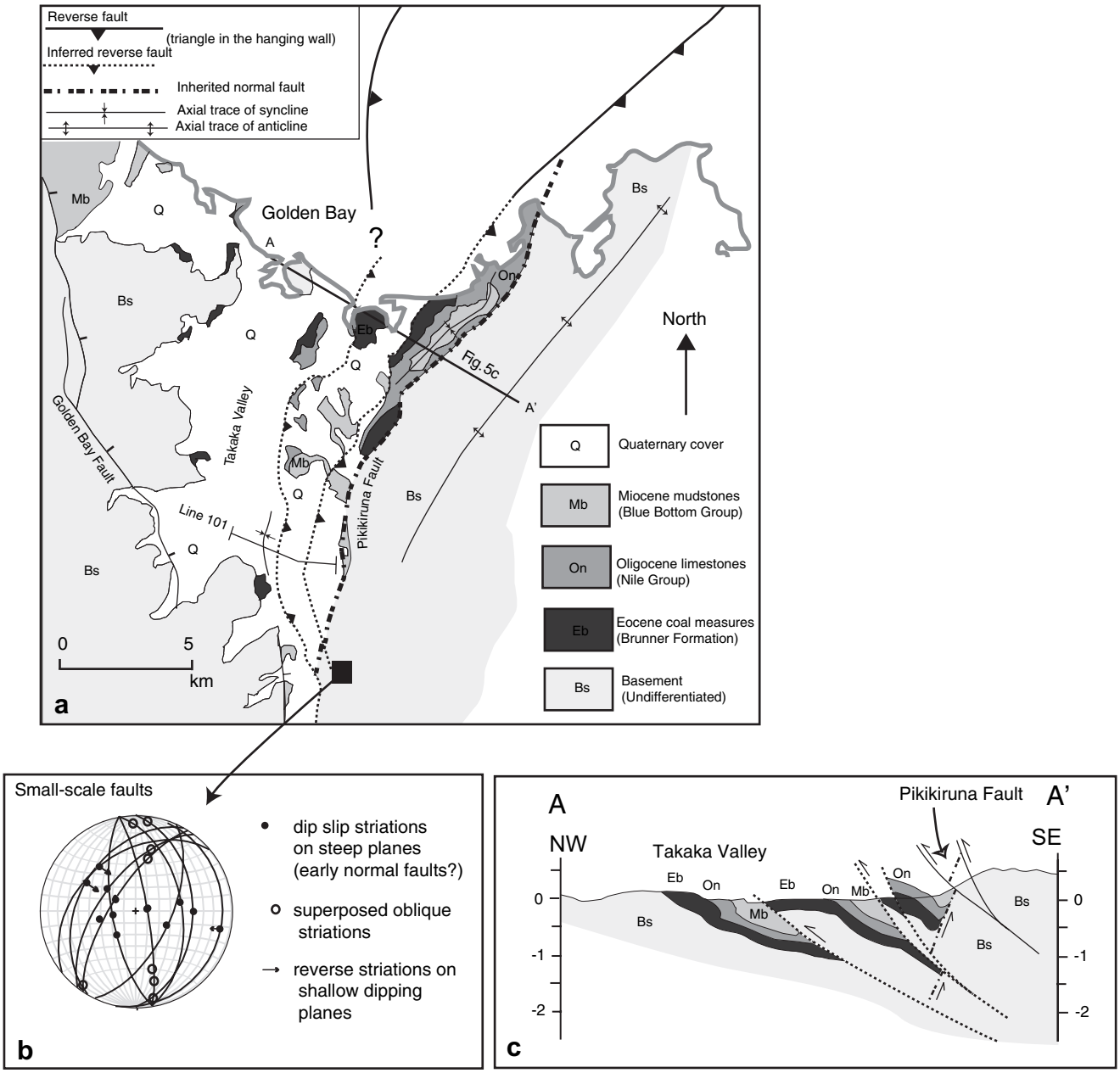

Fig. 5. (a) Geological map (see locality a in Fig. 4a, for regional location), that shows the distribution of the folded and faulted Tertiary sequence in the hanging wall of the high angle Pikikiruna Fault. A set of E-dipping reverse faults identified in the seismic line 101 (Ravens, 1990) is traced north, based on repetition of the Tertiary units. Geology modified from Rattenbury et al. (1998). (b) Small scale structures (lower hemisphere stereographic projection of planes and striations on Schmidt diagram) that indicate the reactivation of dip-slip planes parallel to the Pikikiruna Fault with oblique striations and the cross-cutting of shallow-dipping reverse faults. (c) Cross-section that shows the interpretation of an inherited high-angle Pikikiruna normal fault cross-cut and truncated by E-dipping, low-angle reverse faults.

Mt. William Fault on the east (Fig. 6a and b). Both faults dip away from the surviving portion of the coal basin, truncate syn-depositional NE–SW trending normal faults and NW–SE left-lateral faults within the coal measures (Bishop, 1992b), and—in the case of the Mt. Frederick fault—dip $\leq 30°$. These elements suggest that the early normal faults were not successfully reactivated and were truncated by later, new-formed thrust faults. In other cases (e.g. White Creek Fault, locality c in Figs. 4a and 6c), partitioning of compressional deformation can be identified at outcrop scale, with reverse reactivation of the high angle, inherited normal fault, accompanied by shortening of the footwall through folding, and propagation of new sets of low-angle, conjugate reverse faults.

5. Amount of shortening

Finite shortening of the base of the Oligocene sequence consequent on folding and reverse faulting has been estimated by length restoration along a series of regional transects (Fig. 7). These transects show differential shortening between adjacent areas, but give only a rough estimate of absolute shortening because the relatively stiff Oligocene

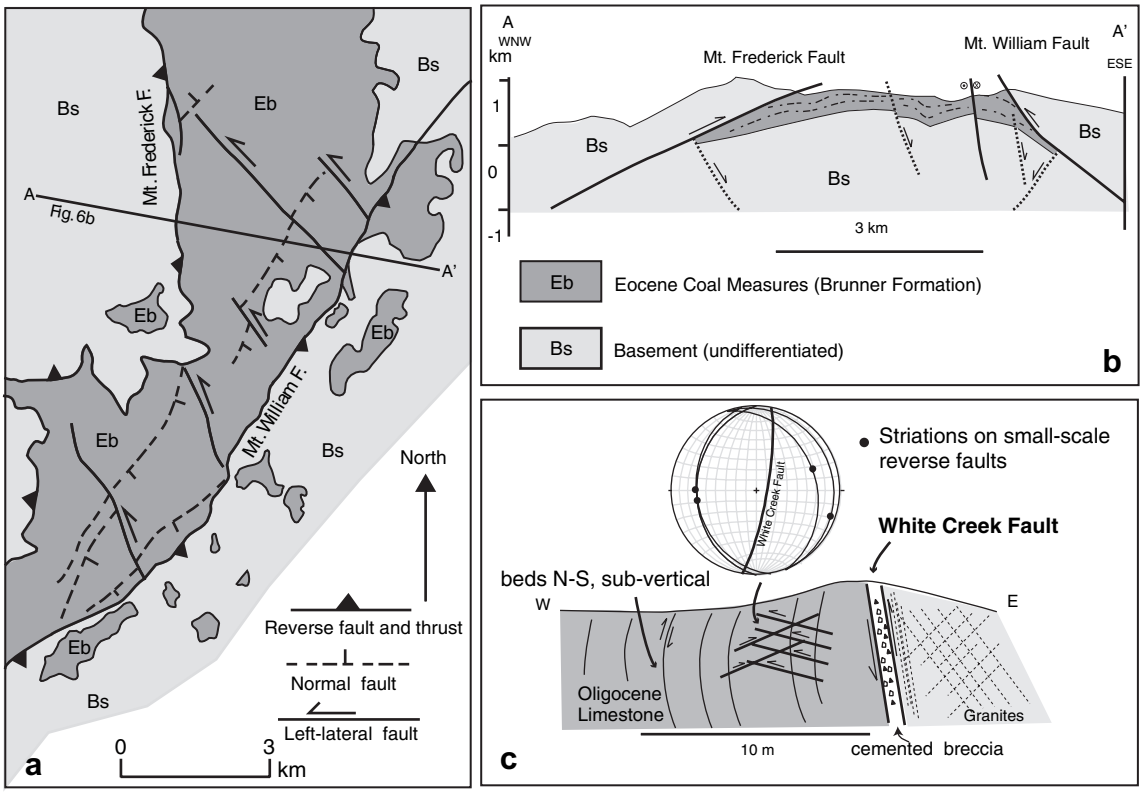

Fig. 6. (a) Geological map (see locality b in Fig. 4a for regional location), that shows the sets of NE–SW and NW–SE high angle normal and left-lateral faults in the Eocene Brunner coal measures, truncated by the W-dipping Mt. Frederick thrust fault and the E-dipping Mt. William reverse fault. Geology modified from Bishop (1992b) and Nathan et al. (2002). (b) Cross-section illustrating the inferred truncation of the Eocene graben during the late stage propagation of cross-cutting reverse faults. (c) Mesoscopic scale structural setting on the White Creek Fault (see locality c in Fig. 4a for regional location). Compressional deformation in the footwall (Oligocene limestones) is partitioned through sets of small scale low-angle reverse faults subparallel to the main, high angle White Creek Fault (lower hemisphere stereographic projection of planes and striations on Schmidt diagram) and bedding-parallel reverse slip. The main fault also shows evidence of reactivation, with reverse striations on a coarse cemented breccia.

limestones overlie highly incompetent Eocene coal measures that may be largely detached above the basement. Fig. 7 shows that shortening is not homogeneously or systematically distributed, and varies significantly along individual transects as well. Shortening >20% is estimated for many transects (1, 2, 4, 5, 6, 7) and the largest values (up to 40%) occur at the eastern ends of transects 4 and 5. Variations could partly be ascribed to lack of detail in the reconstruction of the marker (e.g. central part of transect 2 and all areas close to the Alpine Fault), and to poor resolution on the geometry of faulting at depth, especially if blind thrusts are present. However, large variations in shortening also characterise transects 1, 4, 5, 6, 7, 8, 9, based on higher resolution subsurface information (Janssen, 1963; Petroleum Corporation of New Zealand, 1984; Crundwell, 1990; Ravens, 1990; Bishop, 1992a; Bishop and Buchanan, 1995; Thrasher et al., 1995; New Zealand Oil and Gas, 1997). The estimates shown in Fig. 7 capture differences based on retrodeforming large scale folds and faults along the transects. Significant components of shortening could be added by pervasive deformation (e.g. pressure–solution cleavage), or by large scale layer-parallel detachments. However no systematic correlation is apparent between the distribution of lithological units and the shortening estimates.

The structural style reconstructed for the areas of most intense shortening is shown in the cross-section of Fig. 8. The section takes advantage of detailed surface geology (New Zealand Geological Survey, 1978, 1984, 1990), but data used for depicting geometry of deformation at depth are of inhomogeneous quality. The offshore western part of the section is based on the interpretation of the seismic line EZF-34 (Western Geophysical for ESSO, 1969), published in Bishop and Buchanan (1995). Fault geometry in the area between the Inangahua and Lyell Faults is partially based on the coseismic deformations of the 1968 Inangahua earthquake (Anderson et al., 1994). In the Murchison Basin interpretation uses part of the seismic line MB-01 (Petroleum Corporation of New Zealand, 1984), and the logs of the Murchison-1 (1925–1927), Blackwater-1 (1958) Bounty-1 (1970) and Matiri-1 (1985) wells (see Crundwell, 1990). All the Petroleum Reports on the seismic surveys and boreholes used for the cross-section are in the public domain (stored at Crown Minerals, Wellington, http://www.crownminerals.govt.nz).

The key elements highlighted by this section are:

(1) The existence of inverted, steep faults (e.g. Cape Foulwind Fault) that control the growth of structural highs active during sedimentation of the Plio–Pleistocene sequence.

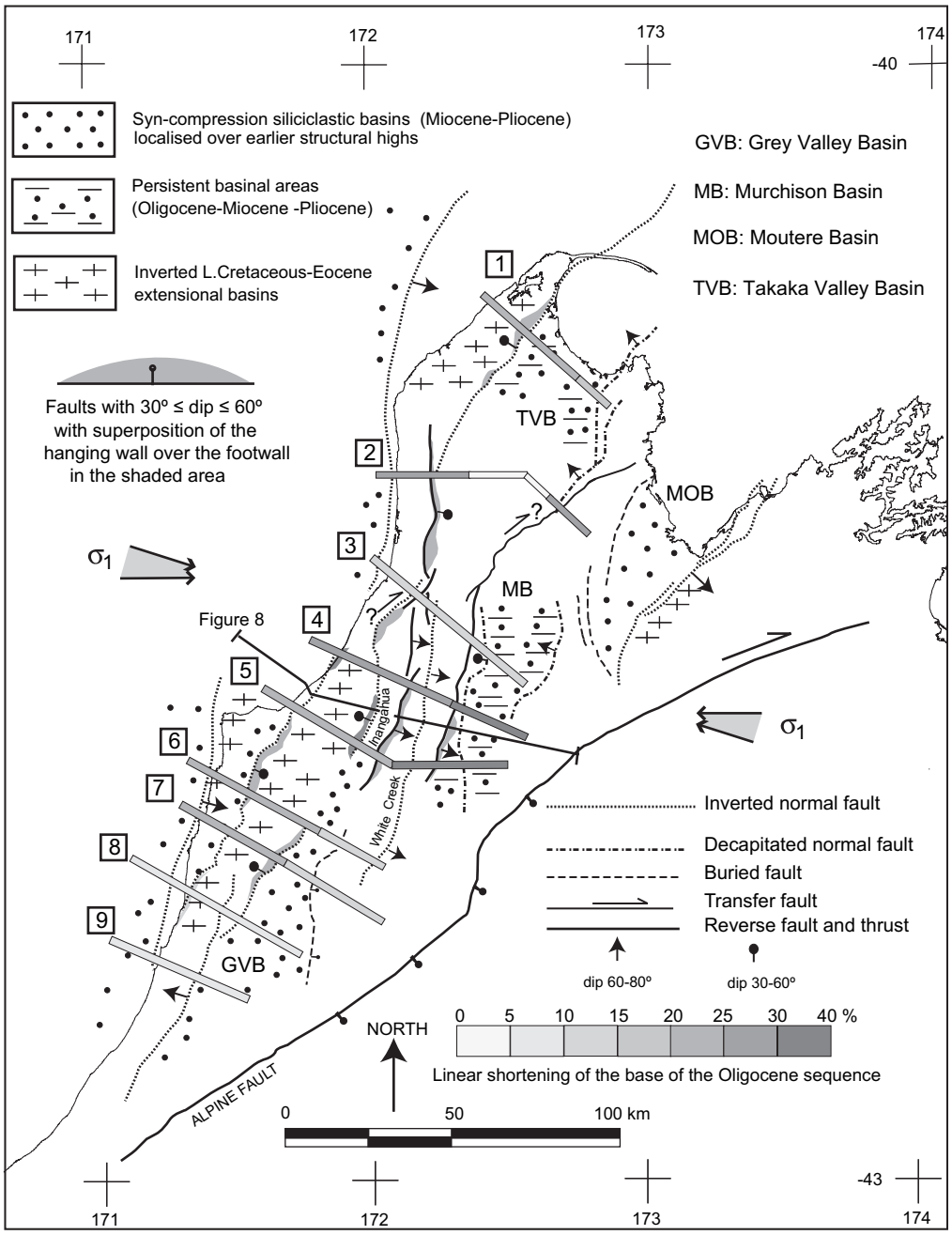

Fig. 7. Regional distribution of inverted extensional basins, syncompressional siliciclastic basins and area of intense shortening relative to the major faults. Linear shortening of the base of the Oligocene sequence has been estimated by restoration along transects 1–9. Range of inferred trajectories of maximum horizontal compressive stress (σ_1) from Nicol and Wise (1992), Pettinga and Wise (1994) and Balfour et al. (2005).

(2) The decapitation of earlier steep normal faults by 30–45° dipping thrust faults (e.g. Matiri Fault in the Murchison Basin, Inangahua Fault) that are inferred to propagate into the basement and—as low angle detachments—within the sedimentary cover. The overthrusting of basement blocks along low-angle thrusts is accommodated in the cover sequence by drape folding, with localisation of syncompressional basins infilled by thick Miocene–Pliocene clastic sequences. This geometry is partly based on the seismic line MB-01 in the Murchison basin, that shows well layered, subhorizontal reflectors (Eocene and Oligocene sequence?) between 1.3 and 2 s TWT, overlain by a poorly reflective upper sequence that correlates with the granitic basement (Karamea batholith) in the footwall of the inverted Maunga Fault (see Crundwell, 1990).

(3) The double vergence imparted by reactivated normal faults and cross-cutting thrust faults, with strong shortening and tectonic uplift in a central, largely denudated area, that separates two Miocene–Pliocene syntectonic troughs that were actively subsiding during the phases of compressional inversion.

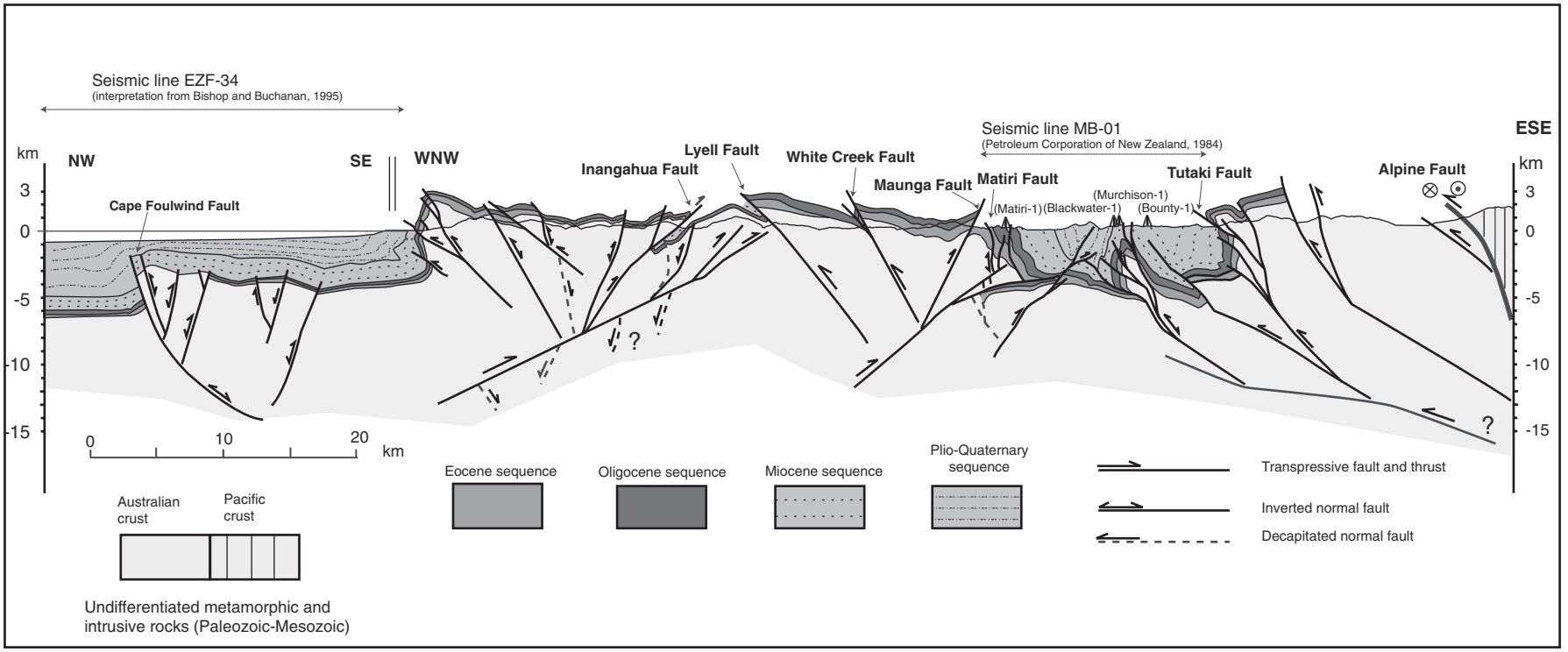

Fig. 8. Regional cross-section (trace in Fig. 5) that illustrates the inferred relationships between steep inverted normal faults and moderate-dipping cross-cutting thrusts. Drill holes in brackets are projected along strike onto the section. Sources of subsurface data are indicated in the figure. Subsurface extrapolation of faults is highly speculative, and addresses the problem of accommodation of shortening underneath the sedimentary cover sequence.

6. Discussion

In the NW of the South Island, increasing convergence between the Australian and Pacific plates and accumulation of right-lateral, transpressive slip on the Alpine Fault started in the Early Miocene. The base of the Oligocene carbonate sequence, deformed by sets of N–S to NNE–SSW folds with subvertical axial surfaces and reverse faults dipping both east and west (Figs. 3 and 4a) is used here to define the style and amount of progressive shortening of the cover sequence overlying the crystalline basement of the Australian crust. At present, the base of the Oligocene sequence has a structural relief of ±3 km relative to the original depositional surface (Fig. 3b and c). Structural highs are areas of net uplift and erosion, whereas structural lows host several thousand metres of Miocene–Pliocene syncompressional clastic sequences that were progressively shortened during the Pliocene and Quaternary. Truncation of fold limbs and steep gradients of the base of the Oligocene sequence occur along interconnected fault systems up to 100 km long (Fig. 4a) that separate domains with contrasting vertical mobility. The mapped geometry of faults, field observations and available seismic lines are indicative of sets of steep (dip $>60°$) and moderate-dipping ($30° \leq$ dip $\leq 60°$) faults (Fig. 4a and c). Although the subsurface geometry of faults remains largely speculative (Fig. 8), a number of geological and seismic data help to constrain the structural style:

(1) The amount of shortening calculated along many transects is >20% and reaches a maximum of 40% in the Murchison Basin (Fig. 7). These values are much higher than the average values previously assessed by Bishop and Buchanan (1995) for the West Coast region (3–4%), but a local shortening of up to 50% was derived by Lihou (1993) from restoration of the folds in the Murchison Basin. Horizontal shortening calculated from retrodeformation of the regional sections in Fig. 7 critically depends on the geometry of folding, on the dip angles of the reverse faults, and on the presence of low-angle thrust faults. The N–S to NNE–SSW faults that are documented to be inherited normal faults reactivated with reverse slip (Fig. 4a) display high-angle dips (45–60°). Most of these faults cause 2–5 km of horizontal shortening, and each of them contributes on average ≤7% to the total shortening of individual transects. Flexural slip folding contributes on average ≤10% (with peaks up to 20%) to the total shortening of each transect. Thrusting on low-angle (20–45°) planes with horizontal shortening of the Oligocene sequence up to 10 km has been inferred for the Murchison Basin, based on the seismic line MB01 (Fig. 8), and this builds up the total shortening along transects 4 and 5 to the estimated 40%.

(2) Evidence for high-angle strike slip faulting is rare. At regional scale, only the NE–SW Karamea and Skeet faults (Fig. 4) show consistent right-lateral displacements of the order of 5–7 km (cf. Rattenbury et al., 1998). Conjugate fault sets with NW–SE orientation and left-lateral mechanisms are locally present, but do not appear to be regionally significant (Fig. 4b). Some field observations suggests that the high angle NW–SE faults are inherited normal faults that underwent left-lateral and oblique reactivation during the compressional episodes (e.g. small scale faults associated with the Pikikiruna Fault in Fig. 5b, and sets of sets of NW–SE left-lateral strike slip faults in the footwall of the Mt. Frederick thrust in Fig. 6).

(3) At regional scale, the compressional inversion of pre-existing normal faults is made evident by the net separation between uplifted extensional basins (Late Cretaceous–Eocene) in the hanging wall and syncompressional Miocene–Pliocene siliciclastic basins in the footwall (Fig. 7). In contrast, persistent subsidence of earlier extensional basins during the Miocene and Pliocene (e.g. Murchison and Takaka Valley basins) is incompatible with reverse reactivation on the same plane of pre-existing normal faults (e.g. Pikikiruna, Maunga, and Matiri Faults).

(4) The area of most intense shortening (Fig. 7) contains the Holocene active fault traces of the Inangahua, Maimai and White Creek Faults. Crustal earthquakes with $M > 4$ since 1962 (Anderson et al., 1993; Doser et al., 1999) define a belt of concentrated activity south of latitude −41°.5, between the coast and the White Creek Fault (Fig. 9). Focal depths range from 8 to 15 km. Unfortunately, poor earthquake locations makes it impossible to identify individual seismic faults, and to detect any systematic westward deepening of focal depths, as predicted by the structural interpretation in Fig. 8. Focal mechanisms (e.g. Anderson et al., 1993; Doser et al., 1999; Reyners et al., 1997; Leitner et al., 2001) show dominant reverse slip on N–S to NNE–SSW trending faults dipping 30–60°, with seismic slip vectors of the largest earthquakes trending on average 260–300°. This trend lies close to the 270–295° range of trajectories of maximum horizontal compression (Fig. 7) reconstructed from structural data (Nicol and Wise, 1992; Pettinga and Wise, 1994) and focal mechanisms (Balfour et al., 2005). Elastic dislocation of the 1929 Buller earthquake has been modelled with a 45° E-dipping thrust (Haines, 1991 in Doser et al., 1999). Coseismic deformation of the 1968 Inangahua earthquake is fitted by a 45° W-dipping, blind thrust fault rather than reactivation of the steeply dipping Inangahua and Lyell faults at the surface (Anderson et al., 1994, see also Fig. 8).

A crude interpretation of the structural relationships is given in Fig. 10. The reconstruction of the Late Cretaceous–Paleocene extensional basins (Fig. 10a) is largely undetermined. The double vergence of the compressional structures is typical of many inverted extensional architectures (e.g. Lowell, 1995), and has been reproduced in a number of experimental models, starting from grabens, half-grabens and domino blocks geometry (McClay, 1995; Yamada and McClay, 2004). In the experiments, propagation of cross-cutting "backthrusts" is observed for increasing amounts of

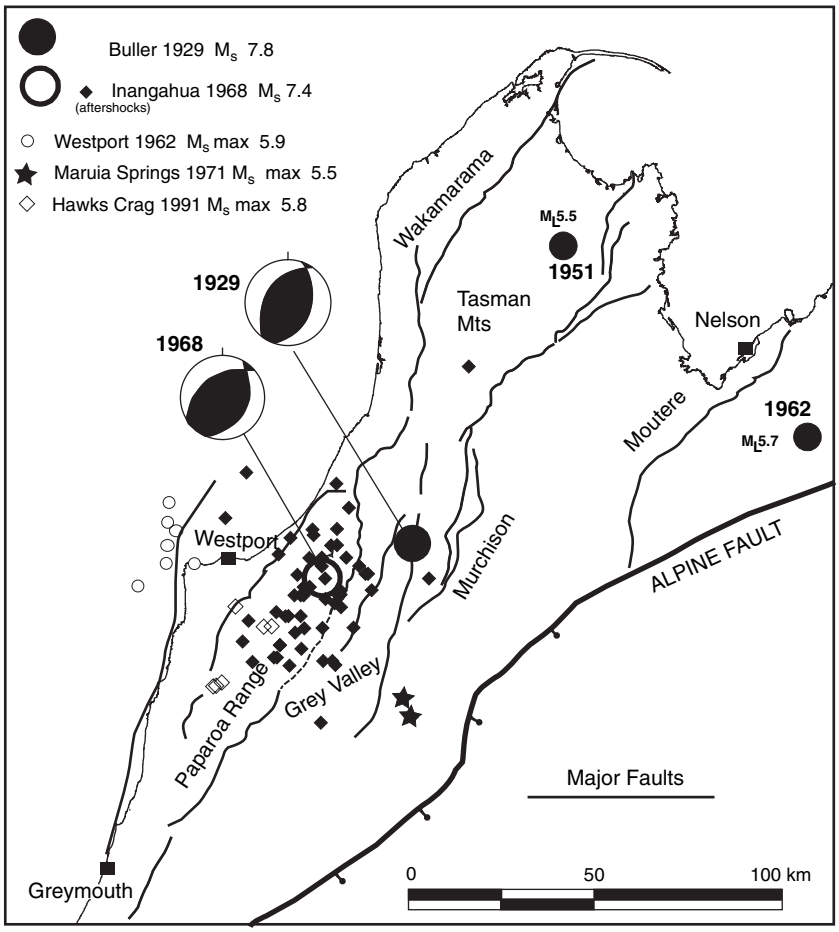

Fig. 9. Location of the major historical earthquakes in the investigated area. Epicentres, magnitudes and focal solutions (lower hemisphere, equal area projections, compressional quadrants in black) after Anderson et al. (1993) and Doser et al. (1999).

contraction, and can be localised by buttressing of a pre-existing flat-ramp geometry within the extensional system (cf. Fig. 10a). However, in the experiments the basement is deformed by only one episode of extension before inversion. In contrast, the basement of this study area has been deformed by a sequence of Paleozoic and Jurassic–Early Cretaceous compressional events, and strong structural and mechanical heterogeneities are imparted by terrane sutures and Paleozoic to Mesozoic magmatic intrusions. Thus, localisation of "new" reverse faults may result from a number of inherited configurations, not uniquely related to the Late Cretaceous–Eocene extensional geometry.

The interpretation suggested in Fig. 10b envisages that active deformation and seismicity are ultimately controlled by moderate-dipping, blind thrust faults that decapitate earlier normal faults. Portions of high-angle normal faults detached in the hanging wall of the cross-cutting thrusts bound rigid basement buttresses that induce steep flexuring of the folded cover sequence. Drape folding above overthrusted basement buttresses (cf. Chester et al., 1988) is accommodated by layer-parallel shears and sub-horizontal detachments. These structures appear to coexist with high-angle inverted faults reactivated with reverse and transpressive motion, and, together, they impart the double vergence to the east and west. The sand-box model of Buchanan (1991) reproduces many characters depicted in Fig. 10, but Bishop and Buchanan (1995) did not recognise in the West Coast of New Zealand the existence of cross-cutting footwall shortcuts that propagate through the basement and decapitate earlier normal faults, as envisaged here. The preponderance of steep and moderate dips in the fault data set and the general lack of low-angle thrusts (dip $<30°$) could result from many of the active reverse faults being composite staircase structures (Fig. 10c) incorporating segments of old, steep normal faults as well as segments of new, lower angle thrusts (cf. the bimodal dip distribution for reverse fault ruptures recognised by Sibson and Xie, 1998).

A major unresolved problem concerns the relationships between active thrusting in the investigated area and the Alpine Fault. The motion between the Australian and Pacific plates in the South Island, with slip rates of 35.5 ± 1.5 mm year^{-1} parallel to the Alpine Fault and 10 ± 1.5 mm year^{-1} perpendicular to it (Fig. 2) has been partly accommodated in the last 5 Ma by transpression on segments of the Alpine fault dipping c. 45° east (Sibson et al., 1979; Norris and Cooper, 1995, 2000), with an estimated 25% of plate-parallel displacement being accommodated away from the fault (Norris and Cooper, 2000). The amount of plate-perpendicular displacement partitioned among other fault systems remains so far unspecified. According to

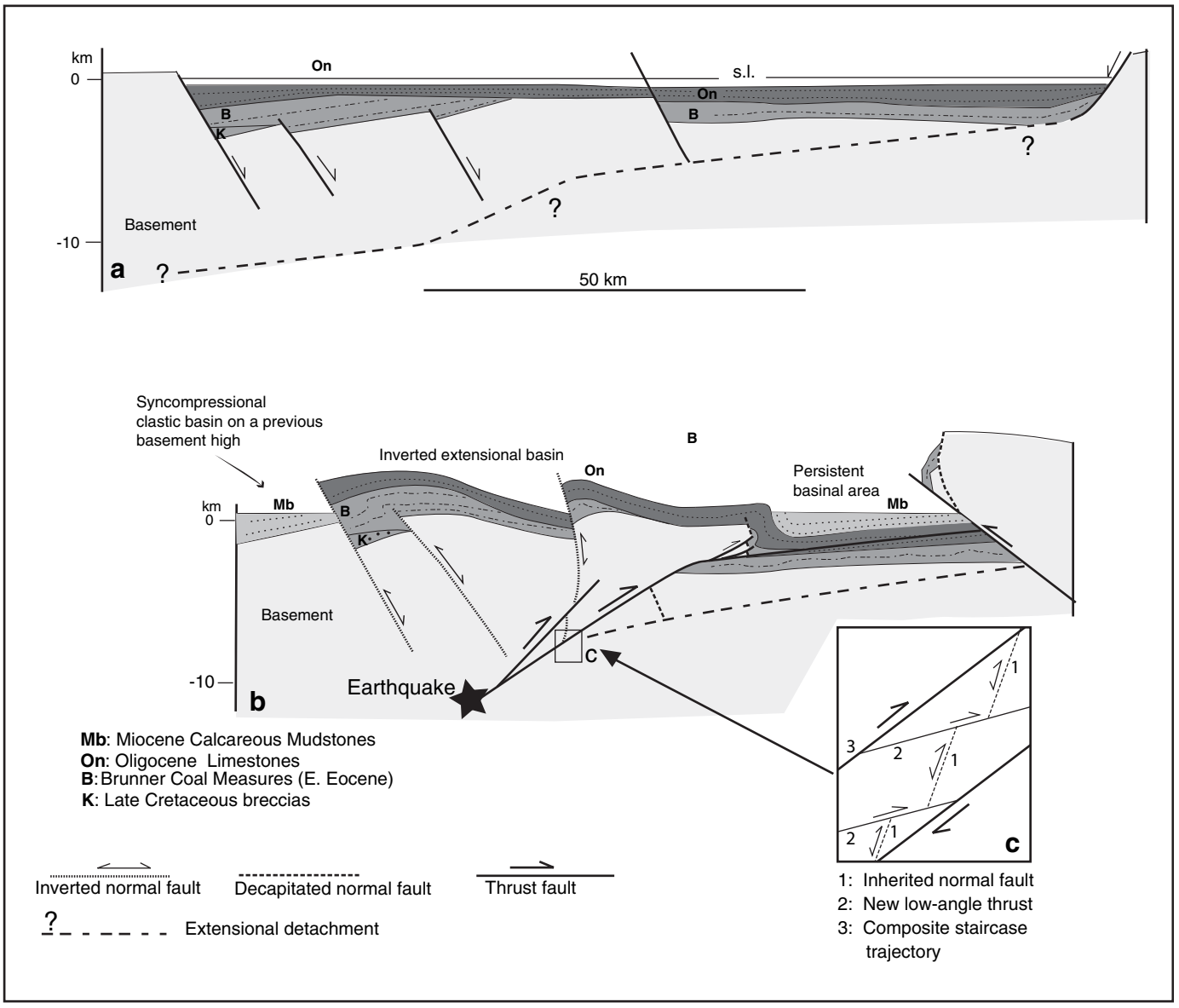

Fig. 10. (a) Schematic cartoon of the inherited geometry of Late Cretaceous–Paleocene extensional basins and normal faults and, (b) deformation resulting from Miocene–Pleistocene shortening, partitioned between compressional inversion of pre-existing normal faults, propagation of moderate-dipping cross-cutting thrusts and flexural folding of the cover sequence. Interpretation is based on field data and available subsurface information. Large magnitude earthquakes at 10–15 km depth are envisaged to be generated by blind thrust faults concealed under detached cover sequences. (c) Composite staircase geometry inferred for the compressional fault structures, comprising portions of steep inherited normal faults and new, low-angle thrusts.

Norris and Cooper (2000), part of it is accommodated in the regions east of the Alpine Fault. However, our data show the intense shortening in the footwall of the Alpine Fault (Fig. 7), in the same area where the structure bends and loses displacement (cf. Anderson et al., 1993). This setting suggests that components of plate perpendicular shortening that are not accommodated on the fault itself are also transferred to footwall shortcut thrusts and backthrusts in the Australian plate.

7. Conclusions

The footwall region of the Alpine Fault in the NW of the South Island is a domain of intense crustal shortening. Convergence has been consistently accommodated over the last 7 Ma by folding and reverse faulting in a network of interconnected N–S to NNE–SSW structures. Reverse faults possess both high angle and low-to-moderate dips and are seismically active in the present compressional stress regime with mechanisms of almost pure reverse slip. Some of the major structures are steep inverted normal faults, inherited from Late Cretaceous–Paleocene extensional phases and some are moderate-dipping thrusts that remain blind and control steep flexuring of the cover sequences. Total finite shortening across the area is too large to be accommodated only by reverse reactivation of the steep faults that are badly oriented in the contemporary stress field and requires slip on low to moderate-dipping thrusts that cross-cut the steep faults, as inferred from field data and seismic profiles. Better subsurface

information will be critical for full analysis of geometrical and timing relationships between reverse faults with different dips.

Acknowledgements

This research was made possible by funding from Geological and Nuclear Sciences, FRST Subcontract C05X0209 ''Earthquake Hazards Assessment from Fault Reactivation Potential in the South Island'', which is gratefully acknowledged. John Taylor and John Barry (Solid Energy New Zealand, Ltd) kindly provided guided access to the coal mining areas in the West Coast. Inputs and criticism from R. Carter, K. Berryman and L. Vezzani were also of great help. R.P. Suggate kindly provided an incisive review when the manuscript was already in press. We also thank John Walsh and an anonymous referee for constructive reviews.

References

Anderson, H., Webb, T., Jackson, J., 1993. Focal mechanisms of large earthquakes in the South Island of New Zealand: implications for the accommodation of Pacific-Australia plate motion. Geophysical Journal International 115, 1032–1054.

Anderson, H., Beanland, S., Blick, G., Darby, D., Downes, G., Haines, J., Jackson, J., Robinson, R., Webb, T., 1994. The 1968 May 23 Inangahua, New Zealand earthquake: an integrated geological, geodetic and seismological source model. New Zealand Journal of Geology and Geophysics 37, 59–86.

Balfour, N.J., Savage, M.K., Townend, J., 2005. Stress and crustal anisotropy in Marlborough, New Zealand: evidence for low fault strength and structure-controlled anisotropy. Geophysical Journal International 163, 1073–1086.

Beavan, J., Haines, J., 2001. Contemporary horizontal velocity and strain rate fields of the Pacific-Australian plate boundary zone through New Zealand. Journal of Geophysical Research 106, 741–770.

Berryman, K.R., 1980. Late Quaternary movement on White Creek fault, South Island, New Zealand. New Zealand Journal of Geology and Geophysics 23, 93–101.

Bishop, J.D., 1992a. Middle Cretaeceous-Tertiary tectonics and seismic interpretation of North Westland and Northwest Nelson, New Zealand. PhD thesis, Victoria University, Wellington, New Zealand.

Bishop, J.D., 1992b. Neogene deformation in part of the Buller Coalfield, Westland, South Island, New Zealand. New Zealand Journal of Geology and Geophysics 35, 249–258.

Bishop, D.J., Buchanan, P.G., 1995. Development of structurally inverted basins: a case study from the West Coast, South Island, New Zealand. In: Buchanan, J.G., Buchanan, P.G. (Eds.), Basin Inversion. Geological Society of London Special Publication 88, pp. 549–585.

Bishop, D.G., Bradshaw, J.D., Landis, C.A., 1985. Provisional terrane map of South Island, New Zealand. In: Howell, D.G. (Ed.), Tectonostratigraphic Terranes of the Circum-Pacific Region. Circum-Pacific Council for Energy and Mineral Resources, Earth Science Series 1.

Buchanan, P.G., 1991. Geometries and kinematic analysis of inversion tectonics from analogue model studies. PhD thesis, University of London.

Buchanan, J.G., Buchanan, P.G. (Eds.), 1995, Basin Inversion. Geological Society of London Special Publication 88, p. 596.

Carter, R.M., 1985. The mid-Oligocene Marshall paraconformity, New Zealand: coincidence with global eustatic sea-level fall or rise? Journal of Geology 93, 359–371.

Chester, J.S., Spang, J.H., Logan, J.M., 1988. Comparison of thrust fault rock models to basement-cored folds in the Rocky Mountain foreland. Geological Society of America Memoirs 171, 65–73.

Crundwell, M.P., 1990. Hydrocarbon potential of the Murchison Basin: a new working model. New Zealand Petroleum Conference Proceedings, 241–249.

DeMets, C., Gordon, R.G., Argus, D.F., Stein, S., 1994. Effect of recent revisions to the geomagnetic reversal time scale on estimates of current plate motion. Geophysical Research Letters 21, 2191–2194.

Doser, D.I., Webb, T.H., Maunder, D.E., 1999. Source parameters of large historical (1918–1962) earthquakes, South Island, New Zealand. Geophysical Journal International 139, 769–794.

Flandin, M.H., 1967. PR 548, Marine seismic reconnaissance survey – Greymouth offshore, N.Z. Shell International Petroleum, Maatschappij.

Hardenbol, J., Thierry, J., Farley, M.B., Jacquin, T., de Graciansky, P.C., Veil, P., 1998. Mesozoic and Cenozoic Sequence Chronostratigraphic Chart. In: de Graciansky, P.C. (Ed.), Mesozoic and Cenozoic sequence stratigraphy of European Basins. SEPM Special Publication 60.

Holt, W.E., Haines, A.J., 1995. The kinematics of northern South Island, New Zealand, determined from geologic strain rates. Journal of Geophysical Research 100, 17991–18010.

Janssen, F.L., 1963. PR 441, Seismic Survey of the Greymouth area: G.R. 44. Shell BP & Todd Oil Services Ltd.

Kamp, P.J.J., Webster, K.S., Nathan, S., 1996. Thermal history analysis by integrated modelling of apatite fission track and vitrinite reflectance data: application to an inverted basin (Buller coalfield, New Zealand). Basin Research 8, 383–402.

King, P.R., 2000. Tectonic reconstruction of New Zealand: 40 Ma to the Present. New Zealand Journal of Geology and Geophysics 43, 611–638.

King, P.R., Thrasher, G.P., 1996. Cretaceous-Cenozoic Geology and Petroleum Systems of the Taranaki Basin, New Zealand. Institute of Geological and Nuclear Sciences Monograph 13, 244.

King, P.R., Naish, T.R., Browne, G.H., Field, B.D., Edbrooke, S.W., 1999. Cretaceous to Recent Sedimentary Patterns in New Zealand (Compilers). Geological and Nuclear Sciences. Folio Series 1.

Koons, P.O., 1990. The two-sided orogen: collision and erosion from the sandbox to the Southern Alps, New Zealand. Geology 18, 679–682.

Lebrun, J.F., Lamarche, G., Collot, J.Y., 2003. Subduction initiation at a strike-slip boundary: the Cenozoic Pacific-Australian plate boundary, south of New Zealand. Journal of Geophysical Research 108, 2453, doi:10.1029/2002JB002041.

Leitner, B., Eberhart-Phillips, D., Anderson, H., Nabelek, J.L., 2001. A focused look at the Alpine fault, New Zealand: seismicity, focal mechanisms, and stress observations. Journal of Geophysical Research 106, 2193–2220.

Lihou, J.C., 1993. The structure and deformation of the Murchison Basin, South Island, New Zealand. New Zealand Journal of Geology and Geophysics 36, 95–105.

Lowell, J.D., 1995. Mechanics of basin inversion from worldwide examples. In: Buchanan, J.G., Buchanan, P.G. (Eds.), Basin Inversion. Geological Society of London Special Publication 88, pp. 39–57.

McClay, K., 1995. The geometrics and kinematics of inverted fault systems: a review of analogue model studies. In: Buchanan, J.G., Buchanan, P.G. (Eds.), Basin Inversion. Geological Society of London Special Publication 88, pp. 97–118.

Nathan, S., Anderson, H.J., Cook, R.A., Herzer, R.H., Hoskins, R.H., Raine, J.I., Smale, D., 1986. Cretaceous and Cenozoic sedimentary basins of the West Coast Region, South Island, New Zealand. In: New Zealand Geological Survey Basin Studies 1. Department of Scientific and Industrial Research, Wellington, New Zealand.

Nathan, S., Rattenbury, M.S., Suggate, R.P., 2002. Geology of the Greymouth Area (Compilers). Institute of Geological and Nuclear Sciences. Geological Map 12, scale 1:250 000.

New Zealand Oil and Gas, 1997. PR 2298, Westland basin, South Island, New Zealand, PEP 38505, PEP 38506.

New Zealand Geological Survey, 1978. Geological Map of New Zealand, 1:63,360, Sheet S31 and pt. S32 Buller-Lyell. Department of Scientific and Industrial Research, Wellington.

New Zealand Geological Survey, 1984. Geological Map of New Zealand, 1:50,000, Sheet M29 AC, Mangles Valley. Department of Scientific and Industrial Research, Wellington.

New Zealand Geological Survey, 1990. Geological Map of New Zealand, 1:50,000, Sheet L29 BD, Upper Buller Gorge. Department of Scientific and Industrial Research, Wellington.

Nicol, A., Nathan, S., 2001. Folding and the formation of bedding-parallel faults on the western limb of the Grey Valley Syncline near Blackball, New Zealand. New Zealand Journal of Geology and Geophysics 44, 127–135.

Nicol, A., Wise, D.U., 1992. Paleostress adjacent to the Alpine Fault of New Zealand: fault, vein and stylolite data from the Doctors Dome area. Journal of Geophysical Research 97, 17685–17692.

Norris, R.J., Cooper, A.F., 1995. Origin of small-scale segmentation and transpressional thrusting along the Alpine Fault, New Zealand. Geological Society of America Bulletin 107, 231–240.

Norris, R.J., Cooper, A.F., 2000. Late Quaternary slip rates and slip partitioning on the Alpine Fault, New Zealand. Journal of Structural Geology 23, 507–520.

Norris, R.J., Koons, P.O., Cooper, A.F., 1990. The obliquely-convergent plate boundary in the South Island of New Zealand: implications for ancient collision zones. Journal of Structural Geology 12, 715–725.

Petroleum Corporation of New Zealand, 1984. Murchison Seismic Survey, P.P.L. 38044.

Pettinga, J.R., Wise, D.U., 1994. Paleostress adjacent to the Alpine fault: broader implications from fault analysis near Nelson, South Island, New Zealand. Journal of Geophysical Research 99, 2727–2736.

Rattenbury, M.S., Cooper, R.A., Johnston, M.R., 1998. Geology of the Nelson Area. Institute of Geological and Nuclear Sciences. Geological Map 9, scale 1:250,000.

Ravens, J.M., 1990. Shallow seismic reflection surveys in the Takaka valley, northwest Nelson. New Zealand Journal of Geology and Geophysics 33, 23–28.

Reyners, M., Robinson, R., McGinty, P., 1997. Plate coupling in the northern South Island and southernmost North Island, New Zealand, as illuminated by earthquake focal mechanisms. Journal of Geophysical Research 102, 15197–15210.

Sibson, R.H., 1990. Rupture nucleation on unfavourably oriented faults. Seismological Society of America Bulletin 80, 1580–1604.

Sibson, R.H., Xie, G., 1998. Dip range for intracontinental reverse fault ruptures: truth not stranger than friction? Seismological Society of America Bulletin 88, 1014–1022.

Sibson, R.H., White, S.H., Atkinson, B.K., 1979. Fault rock distribution and structure within the Alpine fault zone: a preliminary account. In: Walcott, R.I., Cresswell, M.M. (Eds.), The Origin of the Southern Alps. Bulletin of the Royal Society of New Zealand. 18, 55–65.

Sutherland, R., 1995. The Australia-Pacific boundary and Cenozoic plate motions in the southwest Pacific: some constraints from Geosat data. Tectonics 14, 819–831.

Sutherland, R., 1999. Cenozoic bending of New Zealand basement terranes and Alpine Fault displacement: a brief review. New Zealand Journal of Geology and Geophysics 42, 295–301.

Thrasher, G.P., 1989. Miocene faulting in Tasman Bay, Nelson, New Zealand. New Zealand Geological Survey Record 40, 49–55.

Thrasher, G.P., King, P.R., Cook, R.A., 1995. Taranaki Basin Petroleum Atlas. New Zealand Institute of Geological and Nuclear Sciences, Lower Hutt.

Wellman, H.W., 1949. Geology of the Pike River coalfield, North Westland. New Zealand Journal of Science and Technology 30, 84–95.

Yamada, Y., McClay, K., 2004. 3-D analog modelling of inversion thrust structures. In: McClay, K.R. (Ed.), Thrust Tectonics and Hydrocarbon Systems. American Association of Petroleum Geologists Memoirs. 82, 276–301.

Yeats, R.S., 2000. The 1968 Inangahua, New Zealand and 1994 Northridge, California, earthquakes: implications for northwest Nelson. New Zealand Journal of Geology and Geophysics 43, 587–599.